


Article

TiO₂ Microparticles Incorporation in Coatings Produced by Plasma Electrolytic Oxidation (PEO) on Titanium

Federica Ceriani, Luca Casanova , Luca Massimini, Andrea Brenna  and Marco Ormellese * 

Department of Chemistry, Materials and Chemical Engineering “G. Natta”, Politecnico di Milano, Via Mancinelli 7, 20131 Milano, Italy; federica.ceriani@polimi.it (F.C.); luca.casanova@polimi.it (L.C.); andrea.brenna@polimi.it (A.B.)

* Correspondence: marco.ormellese@polimi.it; Tel.: +39-02-2399-3118

Abstract: This research describes the influence of two types of particles, namely rutile and anatase microparticles (average $d < 5 \mu\text{m}$), on the morphology, structure, and anticorrosive properties of PEO coatings on titanium produced in an alkaline solution based on NaOH and sodium metasilicates. The paper reports the experimental results relating to the study of the influence of the electrical regime and working frequency of the anodizing treatment on the interaction between the particles, the substrate, and the oxide to determine the optimal conditions that favour the incorporation of the particles and the production of a thick oxide. PEO coatings are characterized by using a scanning electron microscope (SEM), energy dispersive spectroscopy (EDS) analysis, and X-ray diffraction (XRD) testing. The electrochemical behaviour is evaluated by free corrosion potential monitoring and electrochemical impedance spectroscopy analysis (EIS) performed in a sulphuric acid solution. The particles are successfully incorporated into the coating under any electrical condition and at any frequency. However, only treatments carried out at 1000 Hz allow the production of coatings that combine a large thickness (up to $50 \mu\text{m}$) and improved anticorrosion behaviour. In contrast, oxide layers produced at 20 Hz and in DC show a quite damaged structure, affecting their anticorrosion behaviour and resulting in lower corrosion potential and impedance values.

Keywords: PEO; titanium; microparticles; rutile; anatase; EIS



Citation: Ceriani, F.; Casanova, L.; Massimini, L.; Brenna, A.; Ormellese, M. TiO₂ Microparticles Incorporation in Coatings Produced by Plasma Electrolytic Oxidation (PEO) on Titanium. *Coatings* **2023**, *13*, 1718. <https://doi.org/10.3390/coatings13101718>

Academic Editor: Philipp Vladimirovich Kiryukhantsev-Korneev

Received: 24 August 2023

Revised: 28 September 2023

Accepted: 28 September 2023

Published: 30 September 2023



Copyright: © 2023 by the authors. Licensee MDPI, Basel, Switzerland. This article is an open access article distributed under the terms and conditions of the Creative Commons Attribution (CC BY) license (<https://creativecommons.org/licenses/by/4.0/>).

1. Introduction

Plasma electrolytic oxidation (PEO) is an electrochemical surface treatment aimed at producing a thick and hard oxide layer on the surface of the treated metal through the application of high voltages leading to the generation of energetic discharges on the surface of the growing oxide [1,2]. Such a treatment could be applied to titanium to improve its corrosion resistance in particularly aggressive environments. In fact, even if titanium is characterized by great corrosion resistance on its own, due to the spontaneous formation of a thin oxide layer on its surface, it may undergo corrosion in deaerated or strongly acidic atmospheres. For this reason, it can be necessary to perform a surface treatment, such as PEO, for the application of titanium, for example, in the chemical or oil and gas industry [3]. The ceramic coating produced through PEO is characterized by the presence of surface features, like pores or cracks depending on the electrolytic solution of choice. For example, if PEO is carried out in acids, the TiO_x surface will be characterized by homogeneously distributed pores with variable sizes depending on the applied current density. On the other hand, PEO carried out in alkaline solutions considering the addition of silicates can promote almost pore-free TiO_x surfaces presenting round protuberances [4]. However, at a high pH, more aggressive plasma events occur, inducing the formation of macro-defects in the form of cracks or isolated holes responsible for a reduction in the corrosion resistance of the treated component, since aggressive substances can quite easily enter the coating through them [5]. In order to further improve the corrosion resistance of PEO coatings

on Ti, a possibility is to add particles to the PEO electrolyte favouring the formation of a less defective structure thanks to particle incorporation in the growing oxide [5]. Particles can be continuously trapped inside the molten oxide or stick on its surface; moreover, pores can act as short-circuit paths favouring the entering of particles into the coating and their accumulation at the interface between the inner and superficial layer of the oxide [6,7]. The incorporation of particles in forming the ceramic coating can be inert or reactive depending on the particle properties (size, chemical and thermal stability, etc.) and the operational parameters (electrolyte composition, applied potential, etc.) [6]. In the case of inert incorporation, the particles maintain their shape and size almost unaltered and can be clearly distinguished in the final oxide [8]. This typically occurs when working with large particles (with diameters in the order of tens of micrometres) having enhanced chemical stability and a high melting point [5,6,8]. On the other hand, when particles are small (below a few hundred nanometres) and with a low melting temperature, reactive incorporation may occur. In this case, particles are melted due to the high temperature (up to 10^3 – 10^4 K), which are locally generated at the discharge sites and could react with other elements of the electrolyte and/or the metal substrate, forming a new phase [8–10]. An additional factor that significantly influences the incorporation of particles into the growing ceramic film is their zeta potential, ζ . This parameter affects both the dispersion of particles in the electrolytic solution and the particles' interaction with the substrate. In fact, if the absolute value of ζ is high, repulsion between particles in solution is large, and the formation of agglomerates is prevented, at least favouring the transport of the latter towards the anode (the treated component) [6,11]. For what concerned the PEO operational parameters and their influence on favouring particle retention, it is found that high duty cycle and low frequency are appreciable parameters, since a longer pulse duration allows the generation of long-lived discharge associated with higher temperatures and larger pores where particles can be thrown in [12]. Concerning the electrolytic solution, one of the most important factors is the pH, which influences the zeta potential: the higher the pH, the lower ζ , so under alkaline conditions, the most used particles show a negative zeta potential, and then their incorporation in the forming oxide is favoured when a DC anodic field is applied or during positive pulses when working in an AC regime [6,11]. Nonetheless, since the beneficial effects of using a cathodic current, during PEO treatment on Ti, are well documented by previous studies [13,14], in this work, the use of a bipolar duty cycle is investigated, finding that it imparts an excellent corrosion resistance to Ti oxide coatings. The main parameter objects of investigation will be the anodization frequency and the type of particles added to the electrolytic bath (anatase and rutile). This strategy will be also a valid route to synthesise thick coatings in very short treatments (320 s), stimulating a considerable industrial relevance.

2. Materials and Methods

2.1. PEO Treatment

PEO treatment was performed on titanium grade 2 (UNS R50400) square samples (10 mm per side, 1.2 mm thick) cut by metal shearing. The samples were polished with silicon carbide paper (120, 320, and 600 mesh) and rinsed with distilled water. A 1 M NaOH aqueous solution with $4 \text{ g}\cdot\text{L}^{-1}$ of sodium metasilicate (Na_2SiO_3) was used as a starting electrolyte to which two types of particles were added: rutile microparticles (average diameter $\leq 5 \mu\text{m}$, purity $\geq 99.9\%$) and anatase microparticles (average diameter $\leq 5 \mu\text{m}$, purity $\geq 99.9\%$), purchased from Sigma-Aldrich, St. Louis, MO, USA. The particle addition aimed to reduce the defectiveness of the PEO coatings and improve their corrosion resistance. TiO_2 particles were chosen to favour the occurrence of reactive incorporation, promoting the generation of uniform and compact oxide layers. According to an initial screening based on a visual inspection of the PEO samples, the selected concentration of microparticles was $5 \text{ g}\cdot\text{L}^{-1}$, for which uniform oxides were obtained. The compositions of the electrolytic solutions are reported in Table 1.

Table 1. Sample labels, electrolytic solution composition, and working frequency (RP = rutile particles, AP = anatase particles).

Label	Base Solution	Additives	Frequency (Hz)
PEO_RS_1000	1 M NaOH	5 g·L ⁻¹ RP + 4 g·L ⁻¹ Na ₂ SiO ₃	1000
PEO_AS_1000		5 g·L ⁻¹ AP + 4 g·L ⁻¹ Na ₂ SiO ₃	1000
PEO_RS_20		5 g·L ⁻¹ RP + 4 g·L ⁻¹ Na ₂ SiO ₃	20
PEO_AS_20		5 g·L ⁻¹ AP + 4 g·L ⁻¹ Na ₂ SiO ₃	20
PEO_RS_DC		5 g·L ⁻¹ RP + 4 g·L ⁻¹ Na ₂ SiO ₃	-
PEO_AS_DC		5 g·L ⁻¹ AP + 4 g·L ⁻¹ Na ₂ SiO ₃	-
PEO_S_1000		4 g·L ⁻¹ Na ₂ SiO ₃	1000

The process was run in a 1 L Pyrex beaker containing 500 mL of a solution continuously stirred with a magnetic anchor at a rate of 600 rpm to promote a homogeneous particle dispersion. A cylindrical activated titanium net was inserted inside the beaker and used as a counter electrode. The PEO treatment was performed using a California Instruments Asterion 751 series AC/DC power source. A forming voltage of 90 V was reached according to a ramp of 320 s considering the DC and AC pulsed regime. For the latter, the applied signal consisted of a duty cycle comprising 60% anodic and 40% cathodic, with a cathodic peak of 7% with respect to the applied voltage during the anodic peak repeated at 20 and 1000 Hz.

2.2. Coating Characterization

The surface of PEO samples was analysed by using scanning electron microscopy (SEM) using a Carl Zeiss EVO 50 VP SEM (ZEISS, Oberkochen, Germany), equipped with a Bruker (Milan, Italy) X-ray spectrometer for energy dispersive spectroscopy (EDS). X-ray diffraction was carried out using a Philips PW3020 goniometer (Milan, Italy) with Cu K_{α1} radiation (1.54058 Å). Electrochemical tests were performed through a Metrohm Autolab PGSTAT(Origgio (VA), Italy). The treated specimens were immersed in a H₂SO₄ 10% *v/v* solution heated to 60 °C. Such a solution aimed to reproduce aggressive conditions that can be encountered in some chemical treatments of metals, for example, during pickling operations. For electrochemical impedance spectroscopy (EIS), a standard three-electrodes cell, with a KCl-saturated silver/silver chloride (SSC) reference electrode (+197 mV/NHE) and an Amel Pt counter electrode, was used. The tests were carried out for a total immersion time of about 2 h, during which six cycles of measurement were performed, to study the evolution in time of the impedances. The applied signal consisted of a sine wave with an amplitude of 10 mV_{rms}, and 10 points per decade of frequency were collected in a window between 10⁵ and 10⁻² Hz. Corrosion potential monitoring was performed with the same reference electrode immersed in the previous solution for 24 h tests.

3. Results

3.1. Morphology, Structure, and Chemical Composition

According to SEM images of the sample surface (Figure 1), all of the produced oxides are characterized by the presence of protuberances homogeneously distributed all over the oxide surface, a result already observed in previous studies when adding to a soda bath silicates and phytic acid [4].

In the case of PEO_RS_1000 and PEO_AS_1000, such formations have a globular shape more pronounced than the other cases, with an average dimension of 32 ± 6.4 and 37 ± 6.7 µm, respectively. The globules are often crossed by pores as a result of the pressure exerted by the gas generated during the treatment. Observing samples prepared at 20 Hz, the protuberances appear flatter particularly if considering PEO_RS_20. This can be related to the kinetics of the process, strongly dependent on the anodization frequency. If low frequencies are used, in fact, gas evolution produced according to parasitic reactions has more time to evacuate the sample, resulting in a flatter surface. Moreover, several small cracks cross the surface of samples prepared with rutile particles at 20 Hz as a result of

the release of thermal stresses. Finally, in the case of coatings produced in the DC regime, apart from globules, it is possible to notice large nodular structures requiring the use of a lower magnification. The porosity of PEO_RS_DC and PEO_AS_DC is reduced, and even the presence of cracks seems to be quite limited. Another feature common to all types of samples is the formation of acicular structures all over the surface. These architectures are particularly abundant on oxides produced working in the DC regime.

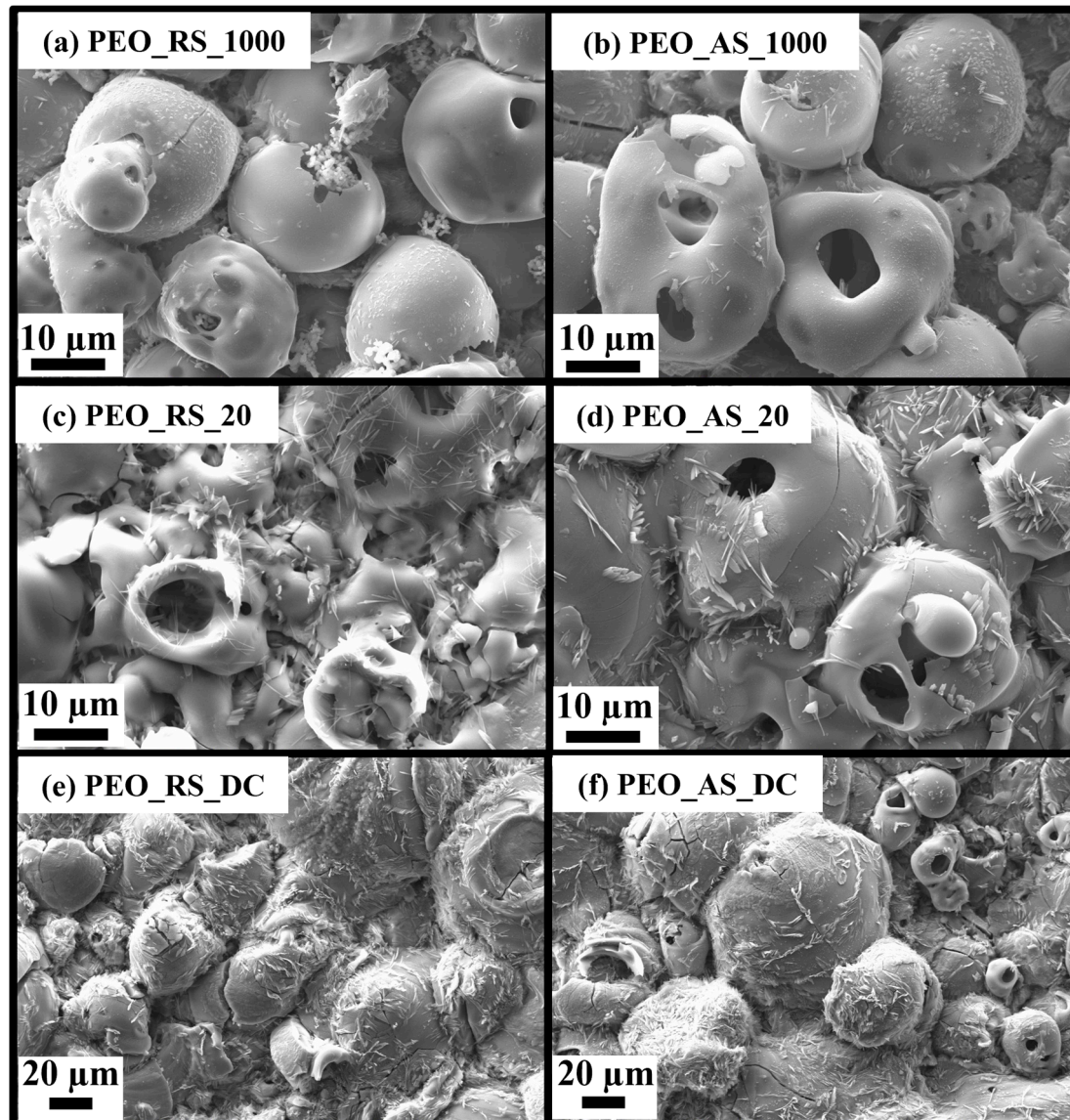


Figure 1. SEM images of surfaces of samples (a) PEO_RS_1000, (b) PEO_AS_1000, (c) PEO_RS_20, (d) PEO_AS_20, (e) PEO_RS_DC, and (f) PEO_AS_DC (notice that different scales are used).

Looking at the cross-sections of the coatings (Figure 2), it is possible to notice that oxides produced at 1000 Hz are quite thick; more precisely, the PEO_RS_1000 and PEO_AS_1000 oxides are $\sim 52.3 \pm 4.6$ and $\sim 49.1 \pm 5.3$ μm thick, respectively. The oxide produced using rutile is characterized by the presence of small pores (the average diameter is reported in Table 2) with a uniform distribution through its thickness, and some larger holes are visible only in the surface layer of the oxide in correspondence with globules. In contrast, PEO_AS_1000 exhibits the presence of large pores in both the inner and outer portions of the coating.

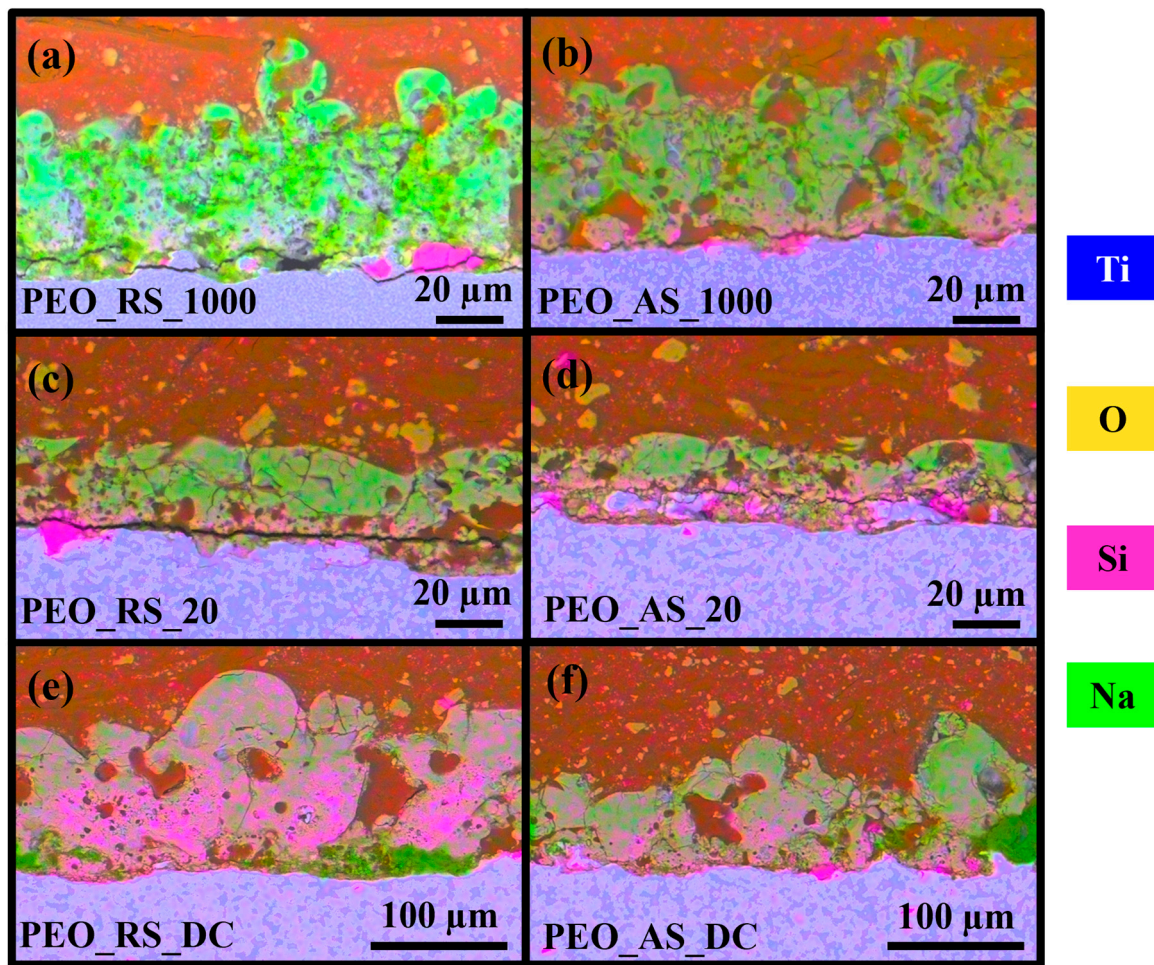


Figure 2. EDS maps of section of samples (a) PEO-RS_1000, (b) PEO-AS_1000, (c) PEO-RS_20, (d) PEO-AS_20, (e) PEO-RS_DC, and (f) PEO-AS_DC (notice that different scales are used). The colour code is titanium in blue, oxygen in yellow, sodium in green, and silicon in pink.

Table 2. Percentage of porosity in the PEO coatings and average pore diameter.

Sample	Porosity %	Average Pore Diameter (μm)
PEO_RS_1000	~28	$\sim 3.1 \pm 2.2$
PEO_AS_1000	~31	$\sim 7.2 \pm 3.7$
PEO_RS_20	~41	$\sim 5.6 \pm 2.6$
PEO_AS_20	~43	$\sim 6.4 \pm 2.7$
PEO_RS_DC	~26	$\sim 23.5 \pm 8.2$
PEO_AS_DC	~35	$\sim 18.9 \pm 9.3$

Oxides produced at 20 Hz are thinner than the previous ones. Working with rutile, an average thickness of $23.1 \pm 3.2 \mu\text{m}$ is obtained, while in the case of anatase, the coating is $\sim 28.0 \pm 2.6 \mu\text{m}$ thick. The PEO_AS_20 appears poorly sintered; in fact, the percentage of porosity for this sample is the highest, especially at the interface with the substrate, while in the outer layers, the oxide seems more compact although large pores are present. PEO_RS_20 appears more compact than its counterpart treated with anatase particles, but also, in this case, large pores are present. It is interesting to notice that for PEO_AS_20, the involvement of the metallic substrate in the PEO process is evident since the oxide penetrates inward in the metal-forming craters and sort of protuberances at the coating–substrate interface. Large discontinuities are also present at the oxide–substrate interface, allowing us to hypothesize a lack of adherence. The SEM images of coating cross-sections also allow

us to better appreciate the difference between the protuberances on samples treated at 1000 Hz, which appear more rounded, and those obtained at 20 Hz, which instead are quite flat. About specimens obtained working in DC, the thickest (PEO_RS_DC $\sim 108.7 \pm 7.2 \mu\text{m}$ and PEO_AS_DC $\sim 81.8 \pm 10.3 \mu\text{m}$) and more compact oxides are produced, especially concerning the one obtained using rutile microparticles in which only some large pores are present.

The EDS analyses (Figure 2) reveal that titanium (in blue), oxygen (in yellow), and sodium (in green) are found in each oxide. Silicon (in pink) presence is also verified for all of the samples, confirming the active role of Na_2SiO_3 in the PEO process where the negatively charged SiO_3^{2-} species is expected to be highly attracted to the anode. Silicon mainly accumulates at the coating–substrate interface, forming sort of agglomerates in all of the PEO coatings, except for PEO_RS_DC, where a quite uniform distribution through the thickness is observed. On the other hand, for such a sample, Na accumulates appreciably only at the interface. This is probably related to the fact that when the anodizing voltage is low, and the first few oxide layers form, the applied field is not enough strong to repel the positively charged Na ions, resulting in a small accumulation at the lower oxide boundary. The contrary holds when the applied potential is strong enough to repel sodium ions from the active region, where new oxide layers are generated, resulting in a sodium-depleted outer region.

To better investigate the influence of the microparticle incorporation morphology of the PEO samples, a comparison between oxides produced at 1000 Hz with and without microparticles was performed. PEO_S_1000 samples (Table 1) were produced using the same electrical parameter described for PEO_XS_1000 samples and by carrying out the treatment in a 1 M NaOH solution containing $4 \text{ g}\cdot\text{L}^{-1}$ Na_2SiO_3 .

In Figure 3, the SEM images of the surfaces of a sample PEO_S_1000 and PEO_RS_1000 are reported.

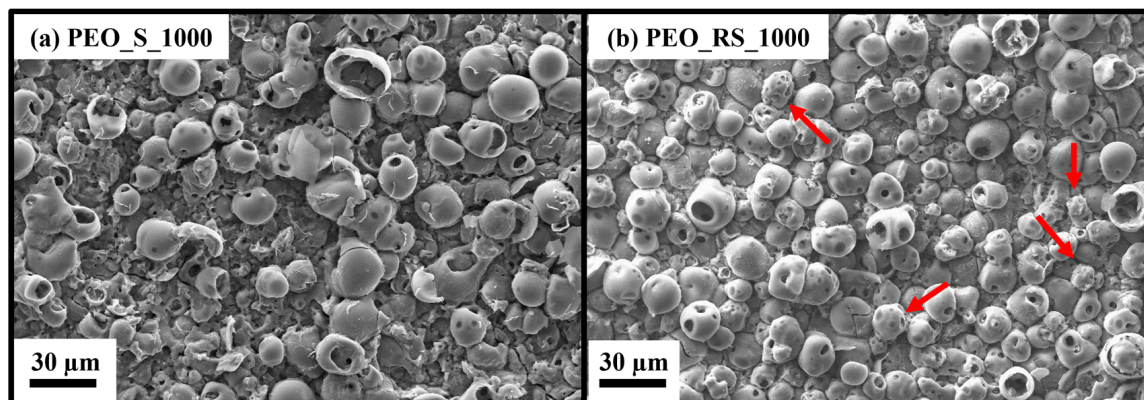


Figure 3. SEM images of surfaces of samples (a) PEO_S_1000 and (b) PEO_RS_1000.

Comparing the two surfaces, it is possible to notice that the globular structures are more abundant and uniformly distributed on the sample treated with MPs, while the surface of PEO_S_1000 appears much more inhomogeneous. Moreover, on the PEO_RS_1000 surface, the presence of spheres (indicated by red arrows) having a morphology slightly different from that of the other globular structure is observed and may result from the agglomeration of MPs with other electrolytic species.

The oxide cross-sections of PEO_S_1000 and PEO_RS_1000 are compared in Figure 4. It is evident how working in the absence of microparticles, a highly inhomogeneous coating is produced, where thicker regions ($>100 \mu\text{m}$) are interrupted by areas where the oxide thickness is reduced to about $20 \mu\text{m}$. This thickness decrease is probably due to the presence at the interface between PEO_S_1000 and the substrate of an oxide layer, which seems characterized by a lack of sintering responsible for the partial detachment of the oxide

external layers. In contrast, the PEO process performed in a solution containing rutile microparticles leads to the formation of a much more uniform coating (Figure 4b).

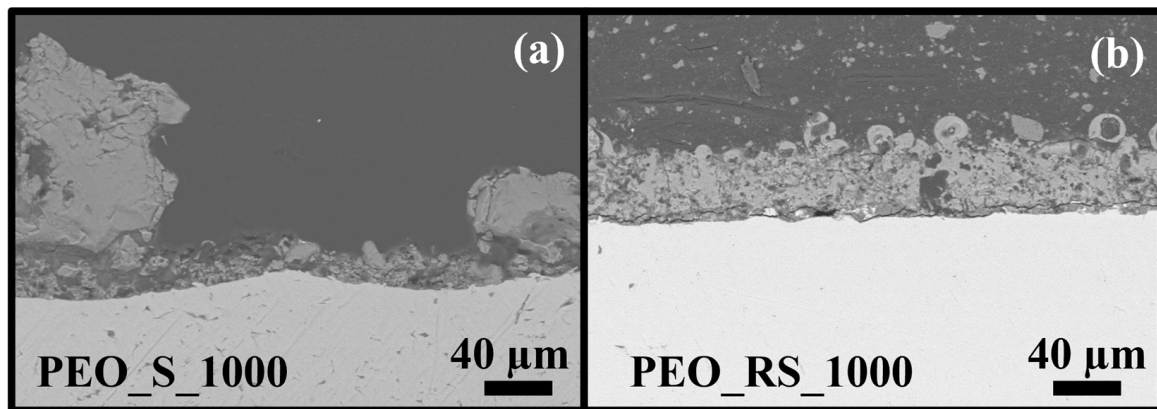


Figure 4. SEM images of cross-sections of samples (a) PEO_S_1000 and (b) PEO_RS_1000.

The XRD analyses (Figure 5) offer a good perspective on the success of particle incorporation.

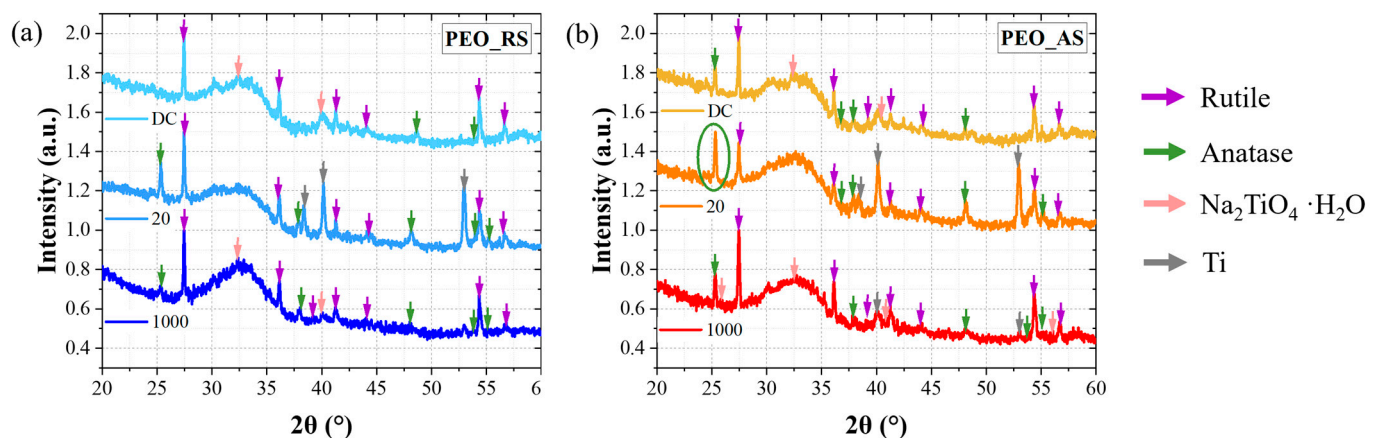


Figure 5. XRD diffractograms of samples (a) PEO_RS_1000, PEO_RS_20, and PEO_RS_DC and (b) PEO_AS_1000, PEO_AS_20, and PEO_AS_DC.

Examining anatase reflections, in fact, it is possible to notice they are almost absent in all of the coatings of the PEO_RS series (apart from small peaks mainly visible for oxides produced at 20 Hz), while they become more numerous and intense for oxides prepared using anatase microparticles. In PEO_AS_20, the anatase peak at 25.34° (circled in green, card number: 98-006-3711) becomes even more intense than the rutile peak at 27.46° (card number 00-001-1292), which, in all of the other samples, is the dominant polymorphic phase. Another peculiarity of oxides produced working at 20 Hz with both rutile and anatase is the presence of quite intense Ti signals. This may be related to the reduced thickness and defective nature of the coatings (observed from SEM images), which allow X-rays to penetrate into the substrate. The XRD also reveals the presence of peaks of sodium titanium oxide hydrate, which are present in all of the oxides except for those treated at 20 Hz. A characteristic common to all of the PEO samples is, instead, the presence in all of the diffractograms of a broad peak around 28 to 35° that is related to the formation of an amorphous material, probably associated with the presence of amorphous silicates and silica [15–19].

3.2. Free Corrosion Potential

Data obtained from corrosion potential monitoring (E_{corr}) are plotted in Figure 6.

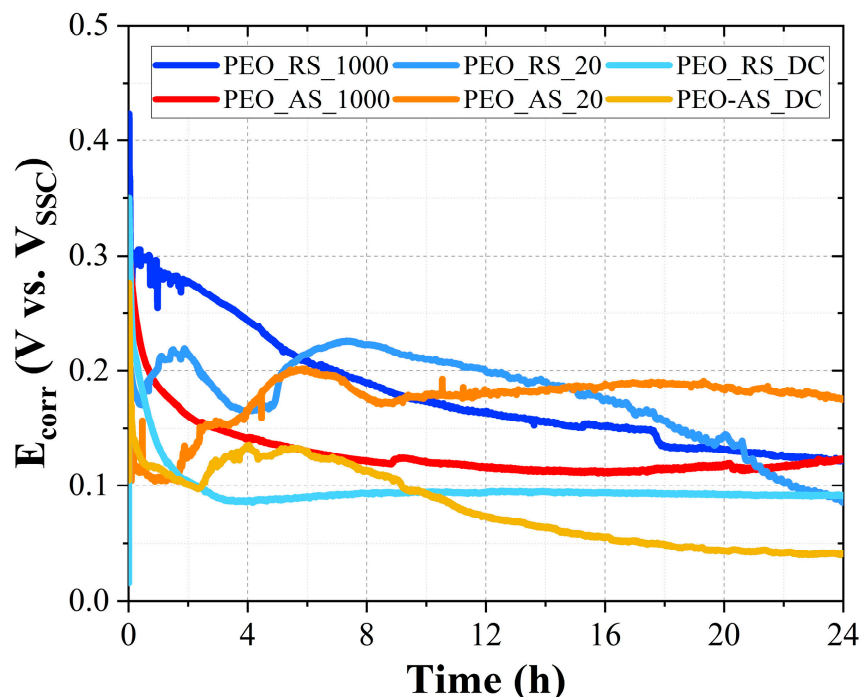


Figure 6. E_{corr} data for 24 h test performed in H_2SO_4 10% v/v at 60 °C.

The PEO treatments increase the nobility of the titanium substrate. All of the anodized specimens, in fact, show a positive E_{corr} ranging between 0.04 and 0.3 V vs. V_{SSC} , while according to [13], shortly after the immersion of Ti Gr. 2 in the aggressive solution, its corrosion potential drops to about -0.48 V vs. V_{SSC} and, after a few hours, stabilizes in the active region at about -0.65 V vs. V_{SSC} (see also Supplementary Materials Figure S1), where abundant hydrogen evolution is detected. Concerning the PEO samples, a rapid decrease in E_{corr} during the first 2–3 h of immersion is observed for all of the samples. After this first step, different trends could be distinguished. The corrosion potential of PEO_AS_1000 remains almost stable for the residual duration of the test as it occurs for PEO_RS_DC, with the difference that the latter shows a lower E_{corr} , meaning that the anodic reaction is slightly more depolarized in this case. PEO_RS_1000 is characterized by a monotonically decreasing E_{corr} even if it presents more noble values for the first 5 h of immersion. The corrosion potential of PEO_RS_20, PEO_AS_20, and PEO_AS_DC after the initial decrease rises to higher values. In the first two cases after the increase, a second drop in E_{corr} takes place, while concerning PEO_AS_20, an average value of ~ 0.183 V vs. V_{SSC} is maintained for the remaining time of the immersion test. After about 16 h of immersion, all of the potentials become stable apart from that of PEO_RS_20, which continues to decrease.

3.3. Electrochemical Impedance Spectroscopy

The impedance data are reported through Nyquist (Figure 7) and Bode (Supplementary Materials Figure S3) diagrams. Polarization resistance values, R_p , are graphically extrapolated from Nyquist diagrams as the intersection of the semicircle fitting the curve with the axis of the real impedances, and the found values are listed in Table 3. In Figure 8, the imaginary impedance is reported as a function of the frequency for only the first and sixth EIS cycles.

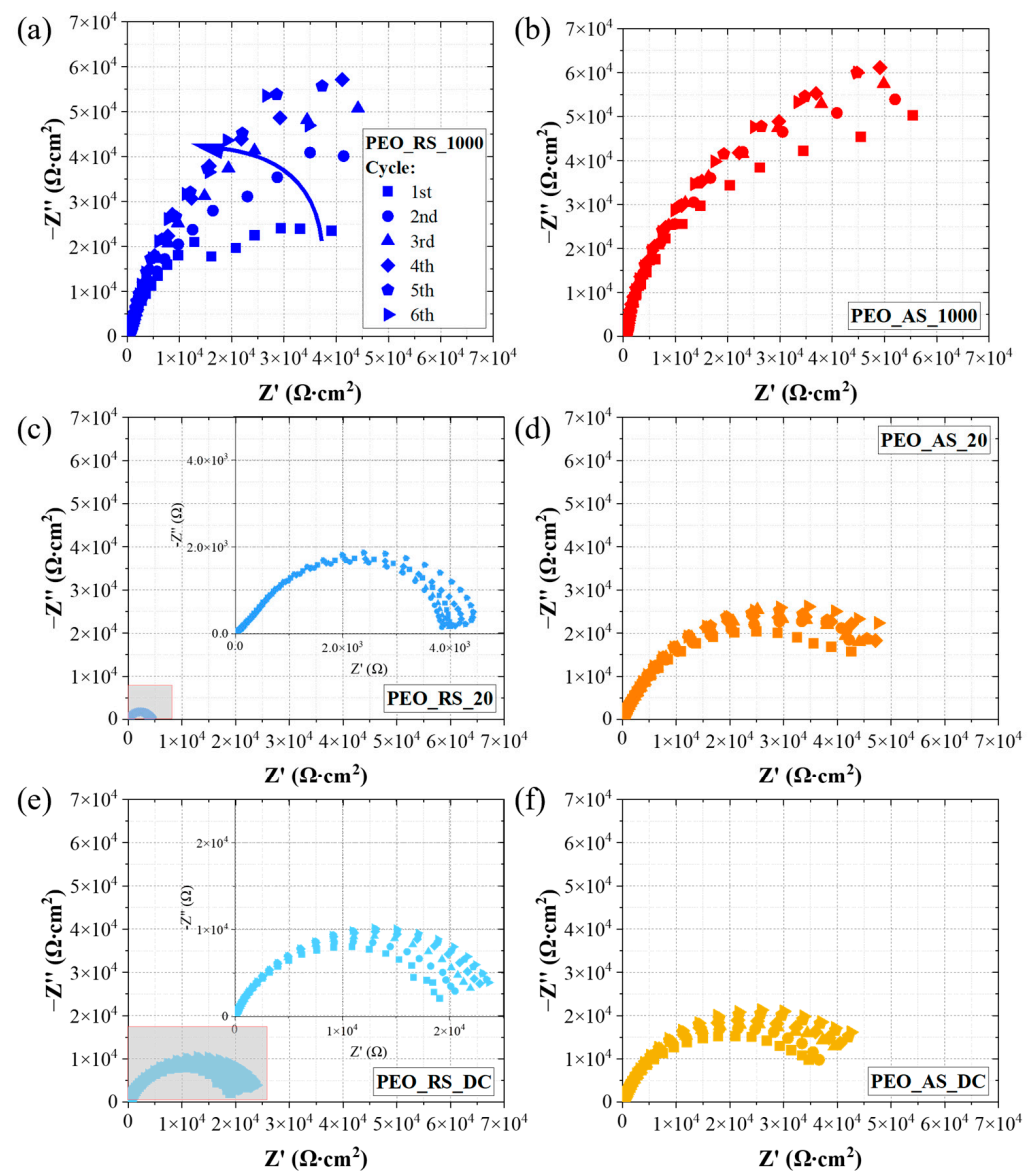


Figure 7. Nyquist diagrams of (a) PEO_RS_1000 (the arrow indicates the time evolution of the Nyquist curves), (b) PEO_AS_1000, (c) PEO_RS_20, (d) PEO_AS_20, (e) PEO_RS_DC, and (f) PEO_AS_DC in H_2SO_4 10 %v/v at 60 °C.

Table 3. Polarization resistance graphically extrapolated from Nyquist diagrams.

Sample	R_p 1st Cycle ($\Omega \cdot \text{cm}^{-2} \cdot 10^5$)	R_p 6th Cycle ($\Omega \cdot \text{cm}^{-2} \cdot 10^5$)
PEO_RS_1000	0.58	1.32
PEO_AS_1000	1.05	1.47
PEO_RS_20	0.04	0.05
PEO_AS_20	0.49	0.64
PEO_RS_DC	0.20	0.25
PEO_AS_DC	0.40	0.52

The electrochemical behaviour of PEO samples appears significantly different from that of bare Ti Gr. 2. The latter, in fact, usually shows a Nyquist diagram with two capacitive loops (Supplementary Materials Figure S2) typical of the ongoing corrosion process controlled by the kinetics of hydrogen evolution [13]. The specimens coated with PEO oxides, instead, show a single capacitive semicircle and impedance values of even

four orders of magnitude higher than uncoated titanium grade 2. These values prove the corrosion protection capabilities of the PEO coatings.

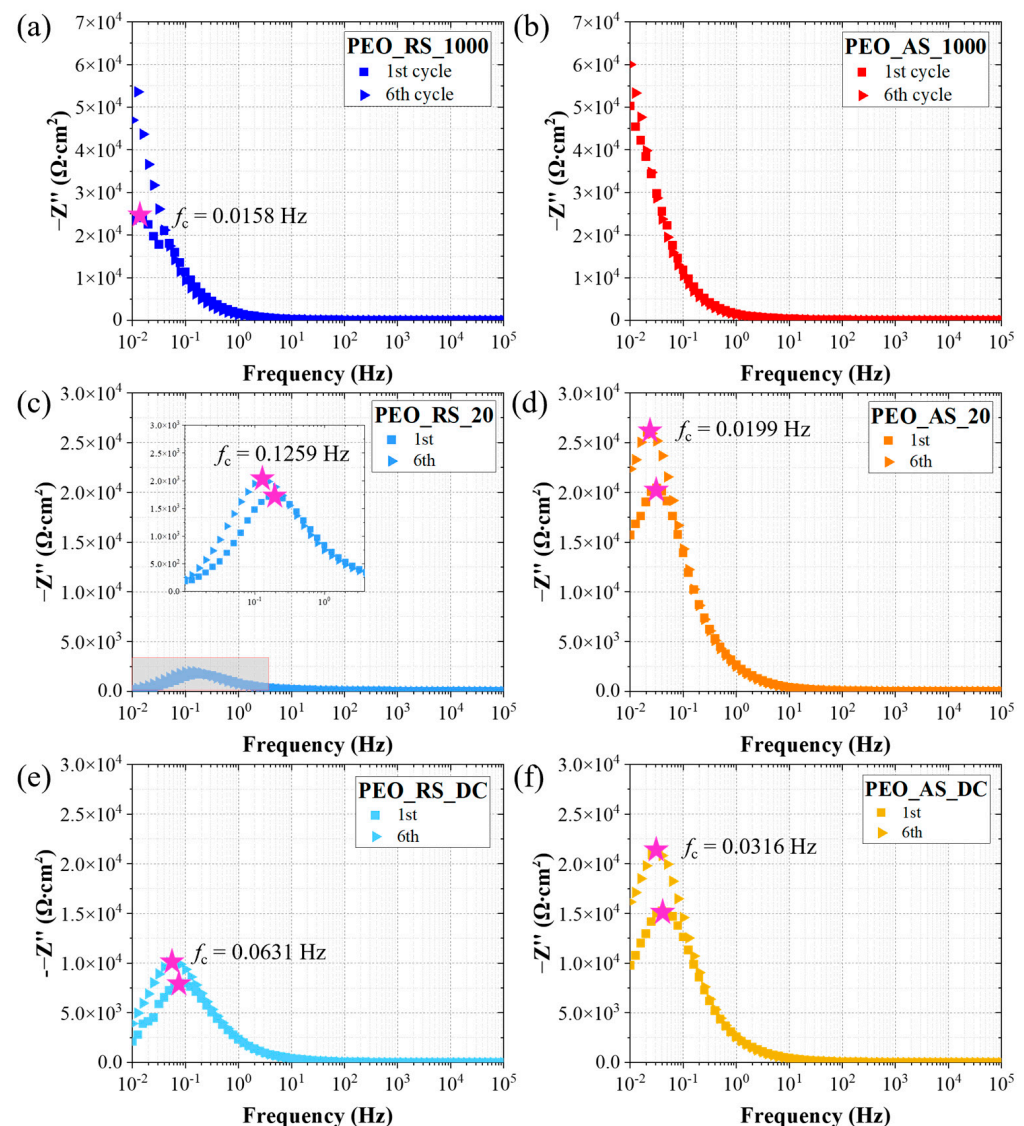


Figure 8. Imaginary impedance of (a) PEO_RS_1000, (b) PEO_AS_1000, (c) PEO_RS_20, (d) PEO_AS_20, (e) PEO_RS_DC, and (f) PEO_AS_DC (a different scale is used for PEO_RS_1000).

Comparing now the diagrams of the different PEO coatings, it is immediately possible to notice the difference between oxides produced at 1000 Hz and the other two types of coatings. Samples treated at higher frequencies show impedance and polarization resistance values significantly larger than those obtained for oxides treated at 20 Hz and DC samples. This is particularly true for PEO_RS_20 whose R_p values are two orders of magnitude lower with respect to those of PEO_RS_1000. This result clearly correlates with the lack of compactness and lower thickness, observed through SEM analysis, obtained according to this formulation.

On the other hand, it is interesting to notice that the time evolution of the electrochemical behaviour of the coatings is the same for specimens produced both in AC and DC. In fact, the diameter of the curves fitting the experimental points of the Nyquist plot increases for subsequent cycles. This increase in impedance is evident especially in the case of PEO_RS_1000 for which $-Z''$ in the final cycle is three times the imaginary impedance of the first cycle.

The same trend over time is noticeable in the Bode diagrams (Supplementary Materials Figure S3), in which, in addition to the impedance values, the phase variation depending on the frequency is reported. PEO_RS_1000, PEO_AS_1000, and PEO_RS_20 show high impedance modulus values at a low frequency, indicating good corrosion resistance and a phase plot characterized by a quite articulated profile, displaying peaks and valleys typical of non-homogeneous electrodes [20]. In contrast, for the other three samples, the phase profile is quite flat and the impedance modulus values are lower, tending to reach a plateau for PEO_RS_20 and PEO_RS_DC, showing lower corrosion resistance.

Concerning the trend of $-Z''$ on frequency (Figure 8), it is observed that for PEO_AS_1000, there are no peaks visible in the experimental window, while PEO_RS_1000 displays a peak at 0.0158 Hz during the first cycle, which moves outside the frequency window in the last cycle. All other oxides show $-Z''$ peaks in the first cycle, which shifts towards a lower frequency in the sixth cycle. The frequencies corresponding to the maximum of the imaginary impedance (named characteristic frequency, f_c) are listed in Table 4 for the first and last EIS cycles.

Table 4. Characteristic frequencies, f_c , of PEO samples for the first and sixth EIS cycles.

Sample	f_c 1st Cycle (Hz)	f_c 6th Cycle (Hz)
PEO_RS_1000	0.0158	$<10^{-2}$
PEO_AS_1000	$<10^{-2}$	$<10^{-2}$
PEO_RS_20	0.1995	0.1259
PEO_AS_20	0.0316	0.0199
PEO_RS_DC	0.0794	0.0631
PEO_AS_DC	0.0398	0.0316

To investigate more deeply the corrosion behaviour of the oxides, Tafel analyses were performed on samples prepared at 1000 Hz (which are those providing the best results in the EIS test). Tafel analyses are performed by polarizing the sample at ± 250 mV with respect to E_{corr} considering a scan rate of $10 \text{ mV} \cdot \text{min}^{-1}$. The Tafel diagrams are displayed in Figure 9, and the data extrapolated from the analysis are listed in Table 5. A comparison with titanium grade 2 is performed.

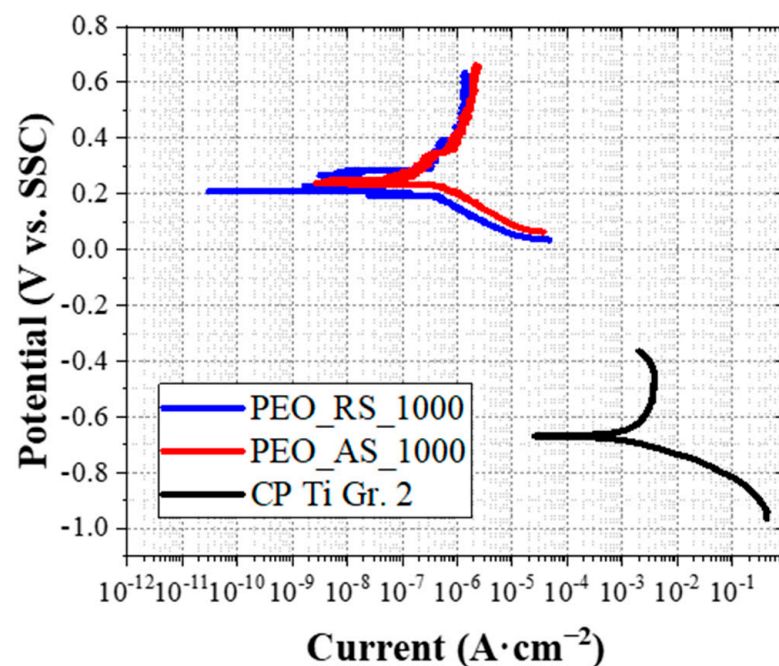


Figure 9. Tafel curves of PEO_RS_1000 (in blue), PEO_AS_1000 (in red), and CP Ti Gr. 2 (in black).

Table 5. Corrosion potential (E_{corr}), corrosion current density (i_{corr}), and anodic and cathodic Tafel characteristics ($|b_a|$ and $|b_c|$) data extrapolated from Tafel analysis.

Sample	E_{corr} (mV vs. SSC)	i_{corr} ($\mu\text{A}\cdot\text{cm}^{-2}$)	$ b_a $ (mV·dec ^{−1})	$ b_c $ (mV·dec ^{−1})
CP Ti Gr. 2	−668	5431	336	754
PEO_RS_1000	209	0.33	541	110
PEO_AS_1000	238	0.59	665	119

PEO_RS_1000 and PEO_AS_1000 show similar behaviour. Both have positive corrosion potential, while that of titanium grade 2 is negative. The corrosion current density of the two PEO specimens is four orders of magnitude lower than that of the untreated metal. The values of $|b_a|$ are slightly higher for the PEO samples with respect to the bare titanium, which can indicate a coating-hindering effect on the anodic reaction. From $|b_c|$ values, it seems that the cathodic reaction (hydrogen evolution) for PEO_RS_1000 and PEO_AS_1000 follows a rather normal kinetics (120 mV of voltage increase for decade of current).

4. Discussion

4.1. Morphology, Structure, and Chemical Composition

The main peculiarity of the structure and morphology of the ceramic coatings is the presence of protuberances on the oxide surface, whose formation can be attributed to the effect of additives containing silicon. In fact, when silicates are added to the electrolytic solution, the final oxide contains SiO_2 in addition to TiO_2 , as highlighted from XRD analyses (Figure 5). Silicon oxide has a higher viscosity than TiO_2 , and consequently, during oxide formation, high-pressure gas bubbles (water vapor, hydrogen, etc.) produced within the oxide remain entrapped by the surrounding molten material. The internal gas could lastly be evacuated from the oxide-forming pores on the globular structures [21,22].

Comparing samples treated in AC and DC conditions, the appearance of the protuberances on the oxide surface is quite different. Such a difference could be explained according to the different kinetics of the electrochemical reactions and the lifetime of plasma events in the two electrical regimes. During DC treatment, static and large discharges are typically generated, which leads to the development of higher temperatures that allow the maintenance of the oxide in a melted state for a longer time, favouring the evacuation of the gas from the forming layer and then the formation of a relatively flatter surface. Moreover, the enhanced gas heating occurring during the DC process influences the dynamics of water vapor diffusion that occurs in a radial direction for longer distances, leading to the generation of larger protuberances [23]. In contrast, in the case of AC processes, the plasma events are generally shorter and smaller than in DC since discharges are suppressed at the end of any anodic half-cycle by the subsequent cathodic part, which also increases the amount of gas produced in the form of H_2 . Consequently, high temperatures are maintained only for a shorter time, promoting the entrapment of the gas, whose flux is controlled mainly by diffusion and convection within the oxide, which can eventually exert a sufficiently high pressure to promote the formation of pores [21,23]. According to these phenomena, it is possible to justify the different levels of porosity across the thickness observed between AC- and DC-produced coatings. When the DC regime is imposed and long-lived and large discharges are produced, huge pores are formed in correspondence with the discharge sites. On the other hand, in the case of AC processes, the shorter and smaller plasma events lead to the generation of small pores uniformly distributed through the oxide and with a round shape as typical for coatings produced using solutions containing metasilicate [9].

Differences are evident even between oxides produced with or without microparticles at 1000 Hz. The latter are locally damaged and poorly sintered, while the former are more homogenous and uniform, which seems to confirm the effect of reducing porosity associated with particle incorporation in the growing film. The different thicknesses of the two kinds of oxides may be explained according to the different current regimes established during the PEO process. Current (I)–time plots (Supplementary Materials Figure S4) were collected

at 300 s of treatment for samples treated at 1000 Hz without and with microparticles. In both cases, the I -time curves were characterized by an initial capacitive I peak due to the electrical double layer (EDL) charging, followed by a smooth decay until a current plateau was maintained for the remaining anodic half-cycle. The plateau formation is related to the ionic contribution of the current, responsible for the oxide growth [24,25]. Since the plateau I value related to the coating produced in the absence of particles (~ 7.5 A) was higher than that of the microparticle-treated sample (~ 2.5 A), it is possible to assume that a higher ionic current contribution allows a larger growth of the former oxide. Unfortunately, the production of a thick coating is completely affected by the poor sintering of its structure, which leads to significant detachments of the external oxide layers, which do not occur for oxides treated with microparticles.

Another difference observed between DC and AC oxides produced with MPs concerns the thicknesses of the PEO coatings. In fact, the thickness of DC oxides is almost twice and three times that of coatings produced at 1000 Hz and 20 Hz, respectively. This significant difference could be due to two main phenomena. First of all, when working in the DC regime, the potential is maintained at a high value for a longer time, while working under AC conditions, a progressive potential rise occurs. It is known from the literature [9,26] that the higher the applied voltage and the longer its application time, the thicker the produced oxide at the expense of the compactness of the structure. This is exactly what is observed when comparing samples treated in AC and DC of the present study. The second reason lies in the fact that TiO_2 particles immersed in an alkaline solution assume a negative zeta potential. According to Lee et al. [27], the isoelectric points (IEP) of rutile and anatase are 6.0–6.5 and 3.8–5.9, respectively. Since the NaOH-based electrolyte used for the PEO process has a pH value higher than these IEPs ($\text{pH} > 14$), the particles will be negatively charged, thus offering the opportunity to be incorporated inside the growing oxide during anodic polarization. Since the anodic phase during the DC process lasts for the entire treatment time, it is reasonable to assume that larger particle incorporation occurs, favouring the achievements of high thicknesses. In contrast, it is quite strange that coatings produced working at 20 Hz are thinner than those obtained at a higher frequency even though at a low frequency, the anodic semi-cycle lasts for a longer time. This fact is probably related to the kinetics of the processes occurring when using a low frequency; in particular, during the cathodic part, intense hydrogen evolution lasting tens of milliseconds may detach a considerable oxide portion but also create a too-alkaline local environment responsible for TiO_2 dissolution. Moreover, rapid cooling of the oxide by the electrolyte where the intense discharges have occurred leads to the release of thermal stresses, forming cracks departing from pores or connecting them and causing the formation of a brittle structure with poor adhesion to the substrate. As a result, when the samples are manipulated for SEM analysis, a partial detachment of the poor sintered oxide may occur, justifying the reduced thickness of the PEO coatings treated at 20 Hz.

Another feature emerging from XRD is the presence of sodium titanates in samples treated in DC and at 1000 Hz. Their formation may be attributed to the alkaline hydrothermal process, which occurs when crystalline TiO_2 is immersed in aqueous NaOH solution [28].

Concerning the elemental distribution defined by means of the EDS analyses, it is interesting to notice how the Si concentration is higher at the interface between the ceramic coating and the metallic substrate (except for PEO_RS_DC). This particular distribution could be justified by the mechanism of SiO_3^{2-} retention into the coating, where the anions enter the oxide through the discharge channels under the action of the strong electric field and accumulate at the bottom of the oxides [22].

A difference between samples treated with electrolytes containing anatase and those containing rutile particles lies in the more porous structure of the specimens of the former. This difference is possibly due to the fact that while the structure of rutile particles remains almost unaltered after the incorporation within the coating, anatase particles probably undergo phase transformation into rutile. Rutile is a high-temperature-phase particle whose

generation is a time-dependent process. During PEO, the high temperature achieved during plasma events may favour the transformation between the two TiO_2 polymorphs [2,29]. This transformation is accompanied by a shrinkage of the crystalline cell (the unit volume changes from 0.1363 to 0.0624 nm³ [30]), which could be responsible for the formation of holes within the oxide layer and for the lower compactness.

The phase transformation is in accordance with XRD data of samples treated with solutions containing anatase particles, for which rutile lines are more intense with respect to the anatase ones (except for PEO_AS_20), which should be justified through the favoured anatase-to-rutile transformation.

Finally, it is possible to notice that particles are not visible on the surface or through the thickness of the final coatings. This suggests that reactive incorporation has taken place, promoted by improved sintering of the TiO_2 particles within the titanium oxide coating due to their equal chemical nature.

4.2. Free Corrosion Potential

Corrosion potential monitoring highlights that all samples have a free corrosion potential more noble than bare titanium. The variation in the E_{corr} values during the first phase of immersion is related to the defective nature (presence of cracks and pores) of the oxide, due to which a few hours are needed for the ion diffusion through the coating to take place and for the potential to stabilize. Thus, the slow reduction in E_{corr} of the PEO coating produced at 1000 Hz with rutile could be explained by the slower ion diffusion in the impervious crystal structure of this TiO_2 polymorph, which limits proton diffusion inside the bulk of the material. The E_{corr} increase observed for specimens produced at 20 Hz, and the DC sample of the anatase series, may be due to the phenomena of dissolution of the oxide followed by the precipitation of products, which may fill the porosity of the coatings, promoting its protective effect.

4.3. Electrochemical Impedance Spectroscopy

The EIS results allow us to immediately distinguish between specimens treated at a high frequency and the other PEO samples. The former show high impedance values that are almost twice those of the other types of coatings. This better behaviour of coatings produced at 1000 Hz during short exposure tests is probably due to the combined effects of the large oxide thickness and the presence of only relatively small pores. Such a structure makes the penetration of the aggressive electrolytic species difficult, offering good protection to the substrate. Samples prepared at 20 Hz, in contrast, are affected by both a reduced thickness and a highly defective structure, which are not able to assure a reliable corrosion-protective effect. Concerning DC samples, their impedance values are low despite the large thickness because of the presence of large pores, which make the penetration of the acidic solution and ionic species into the ceramic coatings quite easy. All samples are characterized by an increase in the impedance values over time. This phenomenon could be explained according to the dissolution–precipitation mechanism already mentioned. This process may involve mainly TiO_2 , resulting in the precipitation of dihydrated titanyl sulphate, $\text{TiOSO}_4 \cdot 2\text{H}_2\text{O}$ [31–33]. This process can lead to the clogging of pores and cracks, improving the protective barrier effect of the coatings. This hypothesis seems to be supported by the fact that the larger increase in impedance values is observed for PEO_RS_1000, which is the oxide showing a finer porosity and a more uniform distribution of Na as highlighted in Figure 2, which then is easier to fill with dissolution–precipitation products.

A further observation concerns the higher impedance values measured for samples treated with anatase with respect to their counterparts containing rutile. This trend is probably related to the larger band gap of anatase with respect to rutile [30], which makes electronic transfer more difficult, increasing the impedance values of PEO oxides containing more anatase. However, it has been verified by previous studies [14,34] that rutile guarantees better acid corrosion behaviour in long exposure tests, probably thanks to its

impervious crystal structure, which limits proton diffusion through the oxide layer, offering more reliable corrosion protection.

Analysing the imaginary impedance versus frequency and the extrapolated characteristic frequencies, it is possible to obtain information about the processes occurring over the surface of the specimens. The presence of only one peak could be related to a single relaxation process. Since the process occurs at low frequencies, it may be controlled by the diffusion of charged species towards the pores and defects in the coatings. In the case of oxides prepared at 1000 Hz, the fine porosity and the quite high thickness make difficult charge penetration, resulting in the absence of peaks in the frequency window. The capability of oxide layers produced at 1000 Hz to limit charge circulation is confirmed also by the reduced values of i_{corr} found from Tafel analyses, which are four orders of magnitude lower than that of titanium grade 2. On the other hand, the defective nature of coatings produced at 20 Hz and in DC allows a slightly faster ion diffusion through the oxide layers, resulting in the $-Z''$ peaks and indicating a lower protection ability of the coatings, especially in the case of the PEO oxide formed at 20 Hz in the presence of rutile particles whose f_c is one order of magnitude higher than that of the other oxides. The shifting of the peaks towards lower frequencies, even outside the experimental window selected, with time can be due to the higher resistance of the oxide caused by the dissolution–precipitation previously explained, which can promote the filling of pores and cracks, reducing charge diffusion.

5. Conclusions

This paper describes the effects of a TiO_2 (rutile and anatase) microparticle addition to the electrolytic solutions used for PEO treatments on titanium with the aim of improving the substrate corrosion resistance tested in an acidic environment.

Particle incorporation occurred according to a reactive mechanism, since no particles were clearly distinguishable in the coating, probably favouring the generation of a more stable and compact oxide. It is observed that in general, the incorporation of microparticles of TiO_2 combined with the use of metasilicates allows us to generate a thick oxide able to protect the metal substrate from corrosion.

Concerning the electrical regime, it is noticed that when working in AC at 1000 Hz, thick oxides with a uniform structure are generated. Such coatings offer the best corrosion protection among those analysed in the paper as highlighted by the electrochemical tests. Performing the PEO treatment at 20 Hz, thin and poor sintering oxide layers are produced. The defective structure of the coatings affects their barrier effect, resulting in quite high characteristic frequencies indicating a faster charge diffusion through the oxide with respect to other coatings. Working in the DC mode, the thickest oxides are produced; however, the generation of highly energetic sparks with a partially destructive nature causes the formation of large defects affecting the protective behaviour of the oxides, which, in fact, show the lowest free corrosion potentials. The two polymorphic types of TiO_2 both provide good corrosion resistance even if slightly higher impedance values are reached when working with anatase due to its larger band gap, which seems to partially compensate for the more defective nature of such coatings with respect to oxides produced using rutile microparticles that show a more uniform structure.

Supplementary Materials: The following supporting information can be downloaded at: <https://www.mdpi.com/article/10.3390/coatings13101718/s1>, Figure S1: Ecorr data of titanium grade 2 for 24 h test performed in H_2SO_4 10% v/v at 60 °C; Figure S2: Nyquist diagram of titanium grade 2 in H_2SO_4 10% v/v at 60 °C; Figure S3: Bode and phase diagrams of (a) PEO_RS_1000, (b) PEO_AS_1000, (c) PEO_RS_20 (different scale), (d) PEO_AS_20, (e) PEO_RS_DC, and (f) PEO_AS_DC in H_2SO_4 10% v/v at 60 °C; Figure S4: Current (I)–time curves at the millisecond time scale of (a) PEO_S_1000 and PEO_RS_1000.

Author Contributions: F.C.: conceptualization, experimental design, data collection, editing, and writing. L.C.: conceptualization, experimental design, data collection, editing, and writing. L.M.: experimental design and data collection. A.B.: conceptualization, experimental design, data collection, editing, and writing. M.O.: conceptualization, experimental design, data collection, editing, and writing. All authors have read and agreed to the published version of the manuscript.

Funding: This research received no external funding.

Institutional Review Board Statement: Not applicable.

Informed Consent Statement: Not applicable.

Data Availability Statement: The data presented in this study are available on request from the corresponding author.

Conflicts of Interest: The authors declare no conflict of interest.

References

1. Sikdar, S.; Menezes, P.V.; Maccione, R.; Jacob, T.; Menezes, P.L. Plasma Electrolytic Oxidation (Peo) Process—Processing, Properties, and Applications. *Nanomaterials* **2021**, *11*, 1375. [\[CrossRef\]](#)
2. Pesode, P.; Barve, S. Surface Modification of Titanium and Titanium Alloy by Plasma Electrolytic Oxidation Process for Biomedical Applications: A Review. *Mater. Today Proc.* **2021**, *46*, 594–602. [\[CrossRef\]](#)
3. Casanova, L.; Gruarin, M.; Pedferri, M.P.; Ormellese, M. A Comparison between Corrosion Performances of Titanium Grade 2 and 7 in Strong Reducing Acids. *Mater. Corros.* **2021**, *72*, 1506–1517. [\[CrossRef\]](#)
4. Casanova, L.; Ceriani, F.; Pedferri, M.; Ormellese, M. Addition of Organic Acids during PEO of Titanium in Alkaline Solution. *Coatings* **2022**, *12*, 143. [\[CrossRef\]](#)
5. Lu, X.; Blawert, C.; Zheludkevich, M.L.; Kainer, K.U. Insights into Plasma Electrolytic Oxidation Treatment with Particle Addition. *Corros. Sci.* **2015**, *101*, 201–207. [\[CrossRef\]](#)
6. Lu, X.; Mohedano, M.; Blawert, C.; Matykina, E.; Arrabal, R.; Kainer, K.U.; Zheludkevich, M.L. Plasma Electrolytic Oxidation Coatings with Particle Additions—A Review. *Surf. Coat. Technol.* **2016**, *307*, 1165–1182. [\[CrossRef\]](#)
7. O'Hara, M.; Troughton, S.C.; Francis, R.; Clyne, T.W. The Incorporation of Particles Suspended in the Electrolyte into Plasma Electrolytic Oxidation Coatings on Ti and Al Substrates. *Surf. Coat. Technol.* **2020**, *385*, 125354. [\[CrossRef\]](#)
8. Fattah-alhosseini, A.; Chaharmahali, R.; Babaei, K. Effect of Particles Addition to Solution of Plasma Electrolytic Oxidation (PEO) on the Properties of PEO Coatings Formed on Magnesium and Its Alloys: A Review. *J. Magnes. Alloy.* **2020**, *8*, 799–818. [\[CrossRef\]](#)
9. Aliofkhazraei, M.; Macdonald, D.D.; Matykina, E.; Parfenov, E.V.; Egorkin, V.S.; Curran, J.A.; Troughton, S.C.; Sinebryukhov, S.L.; Gnednikov, S.V.; Lampke, T.; et al. Review of Plasma Electrolytic Oxidation of Titanium Substrates: Mechanism, Properties, Applications and Limitations. *Appl. Surf. Sci. Adv.* **2021**, *5*, 100121. [\[CrossRef\]](#)
10. Shokouhfar, M.; Allahkaram, S.R. Formation Mechanism and Surface Characterization of Ceramic Composite Coatings on Pure Titanium Prepared by Micro-Arc Oxidation in Electrolytes Containing Nanoparticles. *Surf. Coat. Technol.* **2016**, *291*, 396–405. [\[CrossRef\]](#)
11. Fattah-alhosseini, A.; Molaei, M.; Babaei, K. The Effects of Nano- and Micro-Particles on Properties of Plasma Electrolytic Oxidation (PEO) Coatings Applied on Titanium Substrates: A Review. *Surf. Interfaces* **2020**, *21*, 100659. [\[CrossRef\]](#)
12. Lu, X.; Blawert, C.; Mohedano, M.; Scharnagl, N.; Zheludkevich, M.L.; Kainer, K.U. Influence of Electrical Parameters on Particle Uptake during Plasma Electrolytic Oxidation Processing of AM50 Mg Alloy. *Surf. Coat. Technol.* **2016**, *289*, 179–185. [\[CrossRef\]](#)
13. Casanova, L.; La Padula, M.; Pedferri, M.P.; Diamanti, M.V.; Ormellese, M. An Insight into the Evolution of Corrosion Resistant Coatings on Titanium during Bipolar Plasma Electrolytic Oxidation in Sulfuric Acid. *Electrochim. Acta* **2021**, *379*, 138190. [\[CrossRef\]](#)
14. Casanova, L.; Arosio, M.; Hashemi, M.T.; Pedferri, M.; Botton, G.A.; Ormellese, M. Influence of Stoichiometry on the Corrosion Response of Titanium Oxide Coatings Produced by Plasma Electrolytic Oxidation. *Corros. Sci.* **2022**, *203*, 110361. [\[CrossRef\]](#)
15. Aliasghari, S.; Skeleton, P.; Thompson, G.E. Plasma Electrolytic Oxidation of Titanium in a Phosphate/Silicate Electrolyte and Tribological Performance of the Coatings. *Appl. Surf. Sci.* **2014**, *316*, 463–476. [\[CrossRef\]](#)
16. Kamaluddin, H.S.; Basahel, S.N.; Narasimharao, K.; Mokhtar, M. H-ZSM-5 Materials Embedded in an Amorphous Silica Matrix: Highly Selective Catalysts for Propylene in Methanol-to-Olefin Process. *Catalysts* **2019**, *9*, 364. [\[CrossRef\]](#)
17. Wojcieszak, D.; Mazur, M.; Kaczmarek, D.; Poniedzialek, A.; Osekowska, M. An Impact of the Copper Additive on Photocatalytic and Bactericidal Properties of TiO₂ Thin Films. *Mater. Sci. Pol.* **2017**, *35*, 421–426. [\[CrossRef\]](#)
18. Lu, X.; Shih, K.; Li, X.Y.; Liu, G.; Zeng, E.Y.; Wang, F. Accuracy and Application of Quantitative X-Ray Diffraction on the Precipitation of Struvite Product. *Water Res.* **2016**, *90*, 9–14. [\[CrossRef\]](#)
19. Kalapathy, U.; Proctor, A.; Shultz, J. Silicate Thermal Insulation Material from Rice Hull Ash. *Ind. Eng. Chem. Res.* **2003**, *42*, 46–49. [\[CrossRef\]](#)

20. Qin, J.; Shi, X.; Li, H.; Zhao, R.; Li, G.; Zhang, S.; Ding, L.; Cui, X.; Zhao, Y.; Zhang, R. Performance and Failure Process of Green Recycling Solutions for Preparing High Degradation Resistance Coating on Biomedical Magnesium Alloys. *Green Chem.* **2022**, *24*, 8113–8130. [[CrossRef](#)]
21. Zhang, X.; Aliasghari, S.; Němcová, A.; Burnett, T.L.; Kuběna, I.; Šmíd, M.; Thompson, G.E.; Skeldon, P.; Withers, P.J. X-ray Computed Tomographic Investigation of the Porosity and Morphology of Plasma Electrolytic Oxidation Coatings. *ACS Appl. Mater. Interfaces* **2016**, *8*, 8801–8810. [[CrossRef](#)]
22. Dehnavi, V.; Luan, B.L.; Shoesmith, D.W.; Liu, X.Y.; Rohani, S. Effect of Duty Cycle and Applied Current Frequency on Plasma Electrolytic Oxidation (PEO) Coating Growth Behavior. *Surf. Coat. Technol.* **2013**, *226*, 100–107. [[CrossRef](#)]
23. Yue, Y.; Exarhos, S.; Nam, J.; Lee, D.; Linic, S.; Bruggeman, P.J. Quantification of Plasma Produced OH and Electron Fluxes at the Liquid Anode and Their Role in Plasma Driven Solution Electrochemistry. *Plasma Sources Sci. Technol.* **2022**, *31*, 125008. [[CrossRef](#)]
24. Mortazavi, G.; Jiang, J.; Meletis, E.I. Investigation of the Plasma Electrolytic Oxidation Mechanism of Titanium. *Appl. Surf. Sci.* **2019**, *488*, 370–382. [[CrossRef](#)]
25. Rogov, A.B.; Matthews, A.; Yerokhin, A. Role of Cathodic Current in Plasma Electrolytic Oxidation of Al: A Quantitative Approach to in-Situ Evaluation of Cathodically Induced Effects. *Electrochim. Acta* **2019**, *317*, 221–231. [[CrossRef](#)]
26. Quintero, D.; Galvis, O.; Calderón, J.A.; Castaño, J.G.; Echeverría, F. Effect of Electrochemical Parameters on the Formation of Anodic Films on Commercially Pure Titanium by Plasma Electrolytic Oxidation. *Surf. Coat. Technol.* **2014**, *258*, 1223–1231. [[CrossRef](#)]
27. Hyoun, G.L.; Zuo, J.M. Growth and Phase Transformation of Nanometer-Sized Titanium Oxide Powders Produced by the Precipitation Method. *J. Am. Ceram. Soc.* **2004**, *87*, 473–479. [[CrossRef](#)]
28. Li, M.J.; Chi, Z.Y.; Wu, Y.C. Morphology, Chemical Composition and Phase Transformation of Hydrothermal Derived Sodium Titanate. *J. Am. Ceram. Soc.* **2012**, *95*, 3297–3304. [[CrossRef](#)]
29. Durdu, S.; Usta, M. The Tribological Properties of Bioceramic Coatings Produced on Ti6Al4V Alloy by Plasma Electrolytic Oxidation. *Ceram. Int.* **2014**, *40*, 3627–3635. [[CrossRef](#)]
30. Hanaor, D.A.H.; Sorrell, C.C. Review of the Anatase to Rutile Phase Transformation. *J. Mater. Sci.* **2011**, *46*, 855–874. [[CrossRef](#)]
31. Lasheen, T.A. Hydrometallurgy Soda Ash Roasting of Titania Slag Product from Rosetta Ilmenite. *Hydrometallurgy* **2008**, *93*, 124–128. [[CrossRef](#)]
32. Dubenko, A.V.; Nikolenko, M.V.; Aksenenko, E.V.; Kostyniuk, A.; Likozar, B. Mechanism, Thermodynamics and Kinetics of Rutile Leaching Process by Sulfuric Acid Reactions. *Processes* **2020**, *8*, 640. [[CrossRef](#)]
33. Casanova, L.; Menegazzo, M.; Goto, F.; Pedferri, M.; Duò, L.; Ormellese, M.; Bussetti, G. Investigating the Activation of Passive Metals by a Combined In-Situ AFM and Raman Spectroscopy System: A Focus on Titanium. *Sci. Rep.* **2023**, *13*, 6117. [[CrossRef](#)]
34. Shokouhfar, M.; Dehghanian, C.; Montazeri, M.; Baradaran, A. Preparation of Ceramic Coating on Ti Substrate by Plasma Electrolytic Oxidation in Different Electrolytes and Evaluation of Its Corrosion Resistance: Part II. *Appl. Surf. Sci.* **2012**, *258*, 2416–2423. [[CrossRef](#)]

Disclaimer/Publisher's Note: The statements, opinions and data contained in all publications are solely those of the individual author(s) and contributor(s) and not of MDPI and/or the editor(s). MDPI and/or the editor(s) disclaim responsibility for any injury to people or property resulting from any ideas, methods, instructions or products referred to in the content.